



Efficient activation of persulfate decomposition by Cu₂FeSnS₄ nanomaterial for bisphenol A degradation: Kinetics, performance and mechanism studies

Lingshuai Kong^a, Guodong Fang^{b,*}, Yufeng Chen^a, Meng Xie^a, Feng Zhu^a, Long Ma^c, Dongmei Zhou^b, Jinhua Zhan^{a,*}

^a Key Laboratory for Colloid & Interface Chemistry of Education Ministry, Department of Chemistry, Shandong University, Jinan, 250100, PR China

^b Key Laboratory of Soil Environment and Pollution Remediation, Institute of Soil Science, Chinese Academy of Sciences, 71 East Beijing Road, Nanjing, 210008, PR China

^c The Testing Center of Shandong Bureau of China Metallurgical Geology Bureau, Jinan, 250100, PR China

ARTICLE INFO

Keywords:

Cu₂FeSnS₄
Persulfate
Bisphenol A degradation
Wastewater
Decontamination

ABSTRACT

In this study, a flower-like Cu₂FeSnS₄ (CFTS) nanomaterial was applied to the activation of persulfate (PS) for the degradation of bisphenol A (BPA) in model industrial wastewater. The efficiency of PS decomposition by CFTS, and the mechanism of contaminant degradation by SO₄²⁻ were investigated. The results revealed that CFTS catalyzes PS decomposition more efficiently than the monometallic Cu/Fe/Sn sulfides and exhibits activity over a wide pH range. Electron spin resonance spectroscopy, X-ray photoelectron spectroscopy, and free radical quenching experiments revealed a tandem synergistic effect between Cu, Fe, and Sn in their quaternary chalcogenide systems upon PS activation. The intrinsic electron transfer between Cu, Fe and Sn, especially the ≡Fe(II)* species formed upon the complexation of Fe(II) by S on the surface of the CFTS, overcomes the inhibition of the M⁽ⁿ⁺¹⁾⁺/Mⁿ⁺ redox cycle. CFTS shows promise as a catalyst for wastewater treatment.

1. Introduction

Product manufacture at the industrial level inevitably requires the use of complex mixtures of chemicals, and the organic pollutants produced during such processes are often discharged into local aquatic systems, having severely negative effects on the environment and human health. Along with their high toxicity, the long-term persistence and bioaccumulation of refractory organic pollutants are severe problems associated with current levels of environmental pollution [1]. Endocrine disruption has been recognized as an important mode of toxicity by the U.S. Environmental Protection Agency, leading to the initiation of the Endocrine Disruptor Screening Program (EDSP). Bisphenol A (BPA) is a representative endocrine disrupting chemical (EDC), and high levels of BPA have been observed in underground water, landfill leachates, dust, and drinking water [2,3].

Sulfate radical-based advanced oxidation processes (SR-AOPs) have attracted significant attention for the treatment of toxic organic compounds including EDCs in wastewater [4–7]. PS (S₂O₈²⁻) generates sulfate radicals (SO₄²⁻), an oxidant with a redox potential of 2.5–3.1 V, that transform organic pollutants to less-toxic and even non-toxic products [8]. SO₄²⁻ reacts with OH⁻ to form hydroxyl radicals ('OH) ($k = 6.5 \times 10^7 \text{ M}^{-1} \text{ s}^{-1}$) under alkaline conditions, resulting in faster

degradation rates [9]. PS can be activated by heat, basic conditions, UV irradiation, transition metal ions, and heterogeneous catalysts [10–13]. Of these, PS activation using heterogeneous catalysis has proved to be ideal owing to its efficiency and the facile recovery and recycling of the catalyst.

Polymetallic oxides such as CuFeO₂, CuFe₂O₄, Mn_{1.8}Fe_{1.2}O₄, and Zn_xCu_{1-x}Fe₂O₄ have been widely studied in efforts to develop high-performance catalysts for sulfate radical generation. These polymetallic oxides typically exhibit superior performances to those of monometallic oxides owing to the synergistic effects between Cu/Mn and Fe [8,14–16]. However, polymetallic sulfides have been much less widely explored for such purposes.

Cu₂FeSnS₄ (CFTS) is one of the most important ores of tin [17]. Furthermore, it has been demonstrated to be an earth-abundant quaternary semiconductor and an alternative material for solar energy conversion with outstanding photovoltaic properties. Accordingly, it has received increasing attention owing to its potential application to water splitting, solar cells, and pollutant degradation [18–20]. It has been reported that Cu(I) and Fe(III) have a synergistic effect in the activation of PS by CuFe-type oxides [15,21,22]. This type of CuFe oxide shows high activity and stability in the activation of PS for pollutant degradation. Accordingly, there may be a positive synergistic

* Corresponding authors.

E-mail addresses: gdfang@issas.ac.cn (G. Fang), jhzhan@sdu.edu.cn (J. Zhan).

effect between the Cu, Fe, and Sn on the surface of CFTS.

In this study, CFTS was synthesized by a hydrothermal method and used as a novel catalyst for PS activation with BPA as the target model contaminant. The reactivity of CFTS was investigated under various conditions and compared with those of other monometallic sulfide catalysts. A tandem synergistic effect between Cu, Fe, and Sn in their quaternary chalcogenide systems for PS activation was observed for the first time, representing a potentially innovative solution for overcoming the inhibition of the $M^{(n+1)+}/M^n$ redox cycle. Furthermore, the mechanistic pathways of SO_4^{2-} and ·OH formation for BPA degradation in the CFTS/PS system were explored by means of X-ray photoelectron spectroscopy (XPS) and electron spin resonance (ESR) analysis.

2. Materials and methods

2.1. Chemicals and materials

Copper(II) chloride dihydrate ($CuCl_2 \cdot 2H_2O$, ≥99%), iron(III) chloride hexahydrate ($FeCl_3 \cdot 6H_2O$, ≥99%), tin(IV) chloride pentahydrate ($SnCl_4 \cdot 5H_2O$, ≥99%), thiourea (NH_2CSNH_2 , ≥99%), potassium persulfate ($K_2S_2O_8$, ≥99.5%), tin(II) chloride dihydrate ($SnCl_2 \cdot 2H_2O$, ≥99wt%), and zinc chloride ($ZnCl_2$, ≥99%) were purchased from Shanghai Sinopharm Chemical Reagent Co., Ltd. Cuprous sulfide (Cu_2S , ≥99%), 5,5-dimethyl-1-pyrroline N-oxide (DMPO, ≥97%), Humic acid (HA, ≥90%), BPA (≥97%), and methanol were obtained from Aladdin Chemical Co., Ltd. All chemicals were used as received without further purification. Deionized water (18.25 MΩ cm) was used to prepare all aqueous solutions.

2.2. Nanocrystal synthesis and characterization

CFTS was prepared by a previously published hydrothermal method [23]. In brief, 2 mmol $CuCl_2 \cdot 2H_2O$, 1 mmol $FeCl_3 \cdot 6H_2O$, 1 mmol $SnCl_4 \cdot 5H_2O$, and 5 mmol NH_2CSNH_2 was mixed in 40 mL deionized water. After the solution was stirred for 30 min it was placed in a 50 mL Teflon-lined stainless steel autoclave. The autoclave was sealed and maintained at 220 °C for 18 h before cooling to room temperature. The resulting solid precipitate was isolated by centrifugation and washed three times with deionized water then ethanol and dried in a vacuum oven at 60 °C for 24 h. The preparation of other catalysts used in this study is detailed in the Supporting Information (Text S1).

The morphological and microstructural details of the samples were revealed by field-emission scanning electron microscopy (FE-SEM, ZEISS Gemini 300). X-ray powder diffraction (XRD) patterns of the catalysts were measured on a Bruker D8 X-ray diffractometer using Cu K α radiation ($\lambda = 0.1542$ nm). The specific surface areas of the catalysts were investigated using the Brunauer-Emmett-Teller (BET) N_2 adsorption-desorption method with a Micromeritics ASAP 2020 instrument. Surface compositions and changes in the chemical state were determined using XPS (ESCALAB 250XI, Thermo Electron Corporation), and the binding energies were calibrated by reference to the C 1s peak at 284.6 eV.

2.3. BPA degradation experiments

The degradation experiments were conducted in the dark in a 100 mL conical flask containing 50 mL of BPA solution (0.1 mM) placed in a thermostatic water bath with magnetic stirring (EMS-40, Shanghai Joyn Electronic CO., Ltd.) at 25 ± 2 °C. The reactions were initiated by adding a desired quantity of PS to a solution with a predetermined pH (adjusted using 0.1 M H_2SO_4 or 0.1 M NaOH) containing the catalyst and BPA. Typically, 50 mg of catalyst and 10 mL of 0.5 mM BPA solution were mixed in 35 mL water. After 2 min of ultrasonic dispersion, the suspension was stirred for 20 min in a dark environment to make the adsorption/desorption equilibrium. Then, 5 mL of 50 mM PS was injected into the conical flask to initiate the reaction. At given time

intervals, 2 mL of the suspension was withdrawn for analysis, mixed with 0.5 mL of ethanol, and filtered immediately through a 0.22-μm syringe filter. The reusability of the system was evaluated by reclaiming the catalyst after the reaction, washing it with ethanol, deionized water, and dichloroethane, drying at 60 °C under vacuum, and using it for the next reaction under similar experimental conditions.

2.4. Analysis

The concentration of BPA was measured by high-performance liquid chromatography (HPLC) (ELITE P1201, China) with a C18 reversed-phase column (5 μm, 4.6 mm × 150 mm). A mixture of methanol/water (70:30, v/v) was chosen as the mobile phase at a flow rate of 1 mL min⁻¹. The detection wavelength used for BPA was 278 nm [24]. DMPO was used as a spin trap agent in combination with a JES-X320 spectrometer (JEOL, Japan) to detect the radicals involved in the reaction. The total organic carbon (TOC) contents of the solution were measured using a TOC analyzer (Shimadzu TOC-V CPN). The change in the $S_2O_8^{2-}$ concentration in the solution were measured by a previously published spectrophotometric method [25]. The concentrations of leached Cu, Fe, and Sn were determined by inductively coupled plasma-mass spectrometry (ICP-MS) (Becton Dickinson, USA).

3. Results and discussion

3.1. Physicochemical characteristics of CFTS nanoflowers

CFTS nanoflowers were prepared via a facile hydrothermal approach in an autoclave using metal salts and thiourea. FE-SEM was employed for morphological characterization of the CFTS nanoflowers (Fig. 1a). The CFTS nanoflowers have an average size of 8 μm and are composed of numerous nanosheets with thicknesses of approximately 90 nm. Fig. 1b shows a typical XRD pattern for the CFTS nanoflowers, and the peaks of CFTS centered at 28.5°, 32.9°, 47.5°, 56.6° and 76.7° match well with the (112), (200), (204), (116) and (316) reflections, respectively, of tetragonal-phase stannite (JCPDS Card No. 44-1476). The elemental mapping and EDS spectra of CFTS confirm the elemental composition of the product. As shown in Fig. 1c, The EDS mapping images reveal the uniform distribution of Cu, Fe, Sn, and S throughout the nanoflowers. Furthermore, the EDS results reveal an atomic ratio of 49.61% C; 26.88 Cu; 13.53% Sn; 9.98% Fe as shown in Fig. 1d, and a calculated atomic Cu/Fe/Sn/S ratio very close to 2.1:0.8:1.1:4.

3.2. Catalytic decomposition of PS by CFTS for BPA degradation

3.2.1. Catalytic performance of CFTS in PS activation for BPA degradation

As shown in Fig. 2a, the use of PS or CFTS alone resulted in BPA degradation rates of less than 14%, indicating that both the adsorption capacity of the CFTS nanoparticles and the intrinsic oxidizing power of PS are negligible under these tested conditions. BPA is degraded in the presence of 1 mM PS and 1 g L⁻¹ CFTS at a very low rate (< 24%). Upon increasing the concentration of PS from 1 to 3 mM, the degradation of BPA is slightly accelerated. However, when the PS concentration is 5 mM, the total degradation of BPA is achieved within 45 min, and when the initial PS concentration is increased from 5 mM to 10 mM, the time required for the total degradation of BPA decreases from 45 to 35 min for 1 g L⁻¹ CFTS. The pseudo-first-order rate constants (k_{obs}) for BPA degradation within 45 min are 0.0083, 0.0418, 0.1106, and 0.1200 min⁻¹ for 1, 3, 5, and 10 mM PS, respectively (Fig. 2b).

Changes in the total organic carbon (TOC) content were monitored to evaluate BPA mineralization efficiency. As shown in Fig. 2c, the TOC decreases markedly from 22.4 to 10.9 mg_{Carbon}/L, while corresponding removal efficiency increased from 7.5 to 46.7% when the PS concentration from 1 to 10 mM, indicating that BPA is mineralized to H_2O and CO_2 in the CFTS/PS system (Fig. 2c) [26,27]. To further test this

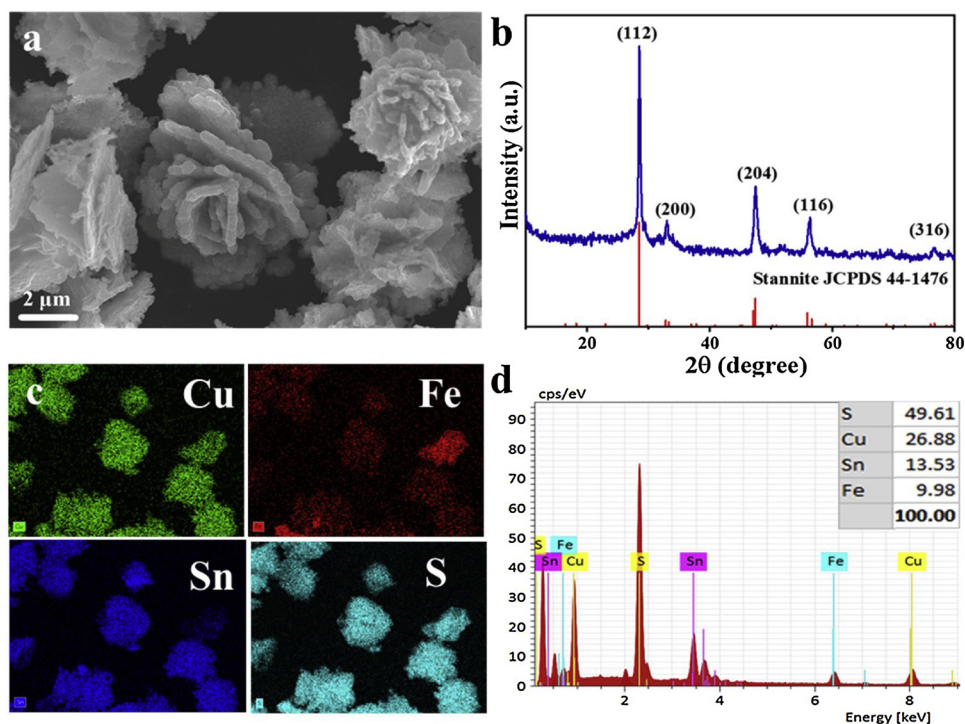


Fig. 1. (a) SEM image of CFTS nanoflowers; (b) XRD pattern of CFTS; (c) FE-SEM EDS mapping images; and (d) EDS spectra of CFTS.

process, the degradation intermediates of BPA were determined by using GC-MS, and the likely pathways of BPA degradation were proposed (Scheme S1). The results show that phenol, 4-isopropylphenol, 4-hydroxyacetophenone, hydroquinone, and glycolic acid were main intermediates of BPA degradation, which can be further oxidized by free radicals to CO_2 and H_2O [26,28]. These combined results suggested that BPA was partially mineralized in the CFTS/PS system, and the generation of more radicals at a high concentration of PS most likely

contributes to the more rapid degradation and mineralization of BPA (Fig. 2d).

Fig. 3 shows that BPA was rapidly degraded by PS (5 mM) with varied CFTS loadings and that the BPA degradation efficiency increased from 17.5 to 100% and the corresponding k_{obs} increased from 0.0050 to 0.2042 min^{-1} when CFTS loading increased from 0.1 to 2 g L^{-1} (Fig. 3b). These results indicated that CFTS was effective at activating PS for BPA degradation, with higher CFTS loadings favoring PS

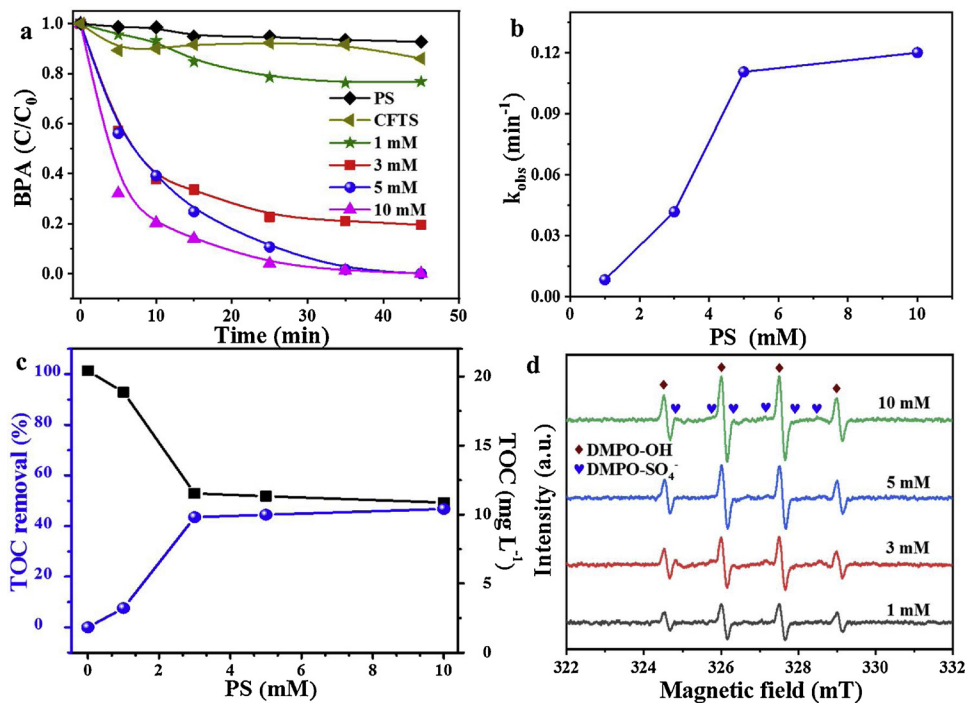


Fig. 2. Kinetics of BPA degradation as a function of PS concentration in the CFTS/PS system: (a) BPA removal efficiency; (b) pseudo-first-order reaction rate constants (k_{obs}); (c) changes in TOC and TOC removal during the reaction; (d) ESR spectra. Reaction conditions: $[\text{BPA}] = 0.1 \text{ mM}$, $[\text{PS}] = 0\text{--}10 \text{ mM}$, $[\text{CFTS}] = 1 \text{ g L}^{-1}$, 25°C .

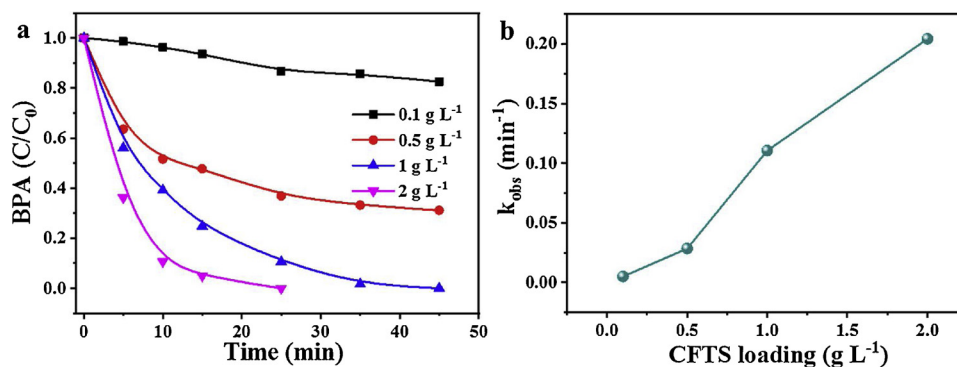


Fig. 3. Degradation of BPA with time as a function of CFTS loading. (a) BPA is rapidly degraded by PS (5 mM) with varied CFTS loadings. (b) k_{obs} as a function of CFTS loading.

activation and BPA degradation. A medium dosage (1 g L⁻¹) with 5 mM PS were used in the subsequent experiments.

3.2.2. Free radical quenching and ESR studies

Free radical quenching studies with tert-butyl alcohol (TBA) and ethanol was usually used to identify the contribution of $\text{SO}_4^{\cdot-}$ and $\cdot\text{OH}$ to pollutant degradation in the sulfate radical-based oxidation processes [29,30], because TBA and ethanol exhibit the similar reaction rate constants with $\cdot\text{OH}$ ($10^8 \text{ M}^{-1}\text{s}^{-1}$). While the reaction rate constants of $\text{SO}_4^{\cdot-}$ with TBA ($10^5 \text{ M}^{-1}\text{s}^{-1}$) was largely lower than that with ethanol ($10^8 \text{ M}^{-1}\text{s}^{-1}$), and thus the efficiency of pollutant degradation would be varied significant when $\text{SO}_4^{\cdot-}$ was the dominant radicals when quencher was in excess. As shown in Fig. 4a, BPA was greatly inhibited with addition of 1 ml TBA or ethanol, but ethanol exerts the greater inhibition effects than TBA due to relatively high reaction rate constants with radicals. With further increasing TBA or ethanol amount to 3 ml, the inhibition effects increased, but changed insignificant when TBA or ethanol amount is increased to 5 ml, which indicated that TBA or ethanol was in excess. The difference in the BPA degradation efficiency between TBA (42.72%) and ethanol (20.83%) was estimated to the contribution of $\text{SO}_4^{\cdot-}$ to BPA degradation, which suggested that $\text{SO}_4^{\cdot-}$ accounted for ~22%, while $\cdot\text{OH}$ was responsible for the ~78% of BPA degradation in the CFTS/PS system. These results indicated that $\cdot\text{OH}$ produced from the reaction of $\text{SO}_4^{\cdot-}$ with H₂O was the dominant radicals for BPA degradation in the present study.

To further identify the active species in the CFTS/PS system, DMPO trapped ESR spectra were used to demonstrate the steady-state concentration of $\text{SO}_4^{\cdot-}$ and $\cdot\text{OH}$. Due to the hyperfine interaction between the electron spins of $\text{SO}_4^{\cdot-}/\text{OH}$ and the orbital spin of the N atom in DMPO, DMPO- $\text{SO}_4^{\cdot-}$ (six lines, 1:1:1:1:1:1) and DMPO-OH (four lines, 1:2:2:1) signals are presented [31]. The ESR spectra of the DMPO- $\text{SO}_4^{\cdot-}$ and DMPO-OH adducts generated in the CFTS/PS system are shown in

Fig. 4b. More $\cdot\text{OH}$ is trapped in the case of the CFTS/PS system in the first 1 min, indicating that $\cdot\text{OH}$ is produced by $\text{SO}_4^{\cdot-}$ reacting with H₂O or OH⁻ [32].

It has been reported that the surface-bound radicals are important reactive species for pollutants degradation in the heterogeneous PS activation processes [33,34]. Therefore, F⁻ was added to determine whether $\cdot\text{OH}$ radicals are generated on the surface of CFTS or in solution via $\text{SO}_4^{\cdot-}$ oxidize H₂O/OH⁻, because F⁻ could desorb $\cdot\text{OH}$ bound to the particle surface by forming hydrogen bond (bound $\cdot\text{OH}$ –F-particle) [35]. The desorbed $\cdot\text{OH}$ can be trapped by DMPO and examined with ESR. As shown in Fig. 5, the addition of F⁻ significantly increases the intensity of DMPO- $\text{SO}_4^{\cdot-}$ signal, demonstrating that the surface-bound $\text{SO}_4^{\cdot-}$ is generated in the CFTS/PS system. However, the intensity of DMPO-OH is decreased in comparison to that for a control experiment, and this can be attributed to F⁻ inhibiting the oxidation of OH⁻ by $\text{SO}_4^{\cdot-}$ on the surface of CFTS by desorbing $\text{SO}_4^{\cdot-}$ and surface hydroxyl bound on CFTS surface. This result suggests that the BPA degraded through a surface catalytic process upon reacting with $\text{SO}_4^{\cdot-}$ and $\cdot\text{OH}$ plays an important role in BPA degradation.

3.3. Effects of pH on BPA degradation in the CFTS/PS system

It is well established that solution pH is an important factor affecting pollutant degradation in PS activation process [32,36]. In the range of pH 3–7, at least 98.6% of the BPA is degraded after 45 min, indicating that CFTS may be performed efficiently for the organic contaminants degradation over a wide pH range (Fig. 6a). This result can be attributable to the fact that Cu rather than Fe plays the major role in the PS activation process under neutral pH condition. Therefore, the CFTS catalytic activation of PS shows a remarkable advantage owing to its flexibility of operating conditions. However, BPA degradation efficiency is decreased to 26% at pH 10, indicating that

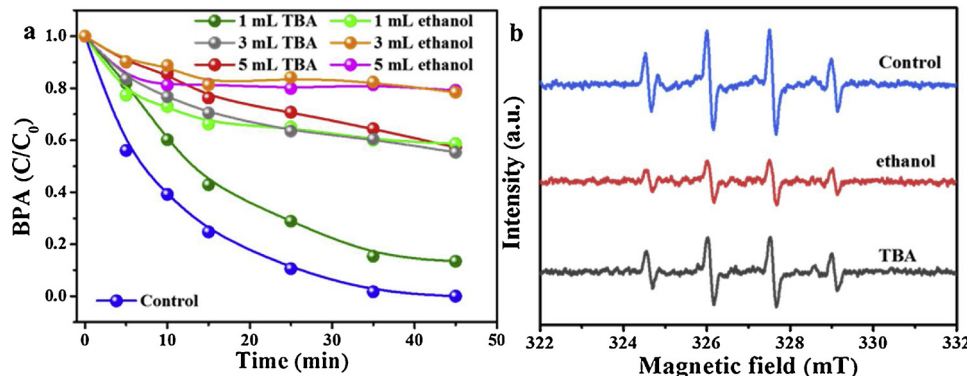


Fig. 4. (a) Effect of radical scavengers on BPA degradation. (b) DMPO spin-trapping ESR spectra obtained from different systems (5 mL ethanol or TBA). Reaction conditions: [PS] = 5 mM, [CFTS] = 1 g L⁻¹, [BPA] = 0.1 mM, 25 °C.

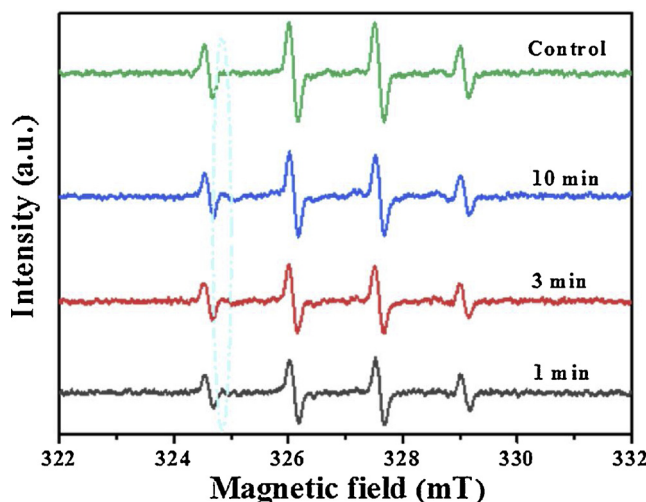


Fig. 5. DMPO spin-trapping ESR spectra obtained at different times in the NaF system (2 mM). Reaction conditions: $[PS] = 5 \text{ mM}$, $[CFTS] = 1 \text{ g L}^{-1}$, 25°C .

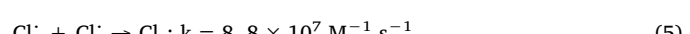
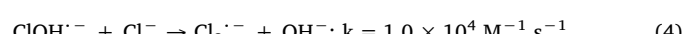
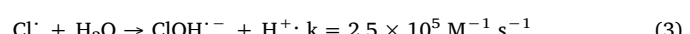
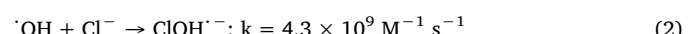
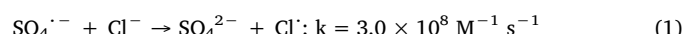
caustic conditions inhibit the degradation of BPA in the CFTS/PS system. $\text{SO}_4^{\cdot-}$ can react with OH^- to form $\cdot\text{OH}$, then the excess $\cdot\text{OH}$ formed can self-quench with $\text{SO}_4^{\cdot-}$ according to the reaction $\text{SO}_4^{\cdot-} + \cdot\text{OH} \rightarrow \text{HSO}_4^- + 1/2 \text{O}_2$, thereby decreasing BPA degradation efficiency [37,38].

3.4. Effects of HA and inorganic ions on BPA degradation in the CFTS/PS system

Humic acid has been extensively selected as model NOM to examine its effect on contaminant degradation in the sulfate radical-based oxidation systems such as nanodiamonds/PS [39], nano-carbon/

peroxymonosulfate [40], UV/oxidants [41]. Therefore, the effects of HA on the kinetics of BPA degradation by the CFTS/PS system was studied (Fig. 6b). The removal efficiency of BPA is clearly decreased by the presence of 1 mg L^{-1} HA in the CFTS/PS system, possibly resulting from the scavenging of $\text{SO}_4^{\cdot-}$ and $\cdot\text{OH}$. However, the BPA removal efficiency only slightly decreases upon further increase the HA concentration. These results indicate that HA inhibits the activation of PS by CFTS by covering the active sites on its surface. Therefore, when applying SR-AOPs, a pretreatment for the removal of organic matter should be considered in order to minimize the negative effects of these non-target compounds.

Chloride ion (Cl^-) is a dominant radical scavenger in wastewater and have been found to have negative effects on BPA degradation [36]. The BPA removal efficiency is slightly decreased when $1\text{--}5 \text{ mM Cl}^-$ is added (Fig. 6c). Cl^- can be converted to other reactive species such as $\text{Cl}_2^{\cdot-}$ (2.09 V) and Cl_2 (1.36 V) upon reaction with $\text{SO}_4^{\cdot-}$ and $\cdot\text{OH}$ (Eqs. (1)–(5)) [42], and these species have much lower oxidation potentials than those of $\text{SO}_4^{\cdot-}$ and $\cdot\text{OH}$. This results in the weakness of the inhibition of the CFTS/PS process by Cl^- observed in this study.



The presence of HCO_3^- or CO_3^{2-} in a water matrix can also decrease contaminant removal efficiency [43,44]. As shown in Fig. 6d, the presence of CO_3^{2-} or HCO_3^- (1 mM) has a significant inhibitory effect, which is ascribed to the strong scavenging of $\text{SO}_4^{\cdot-}$ and $\cdot\text{OH}$ radicals (Eqs. (6)–(9)) [43].

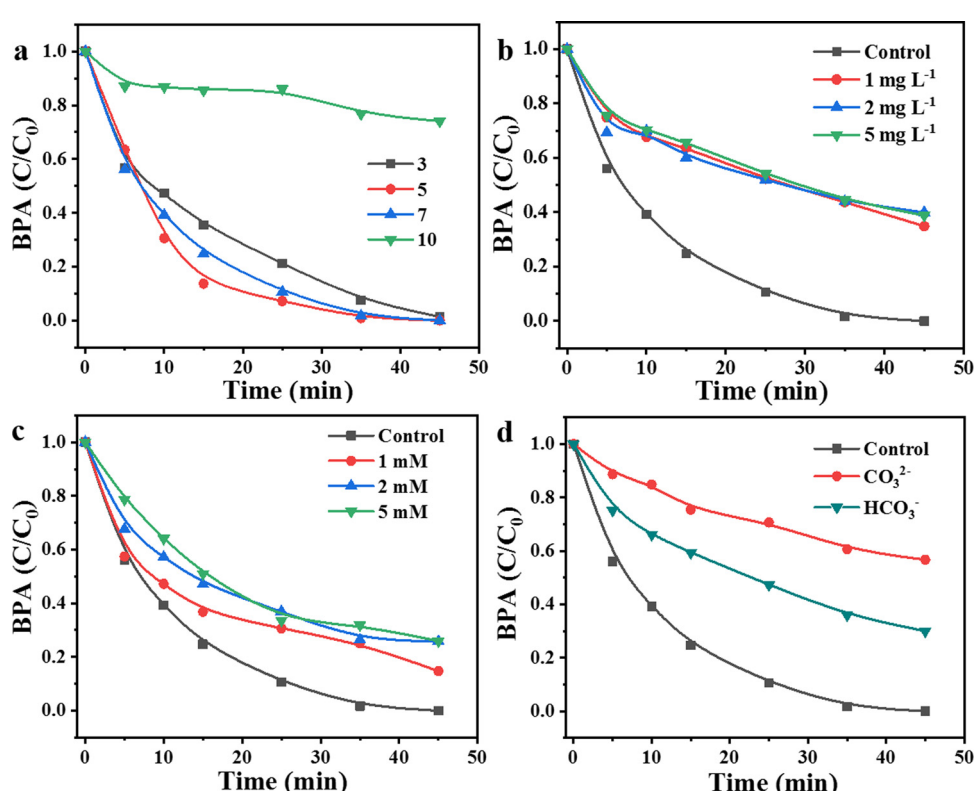
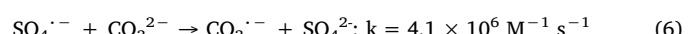
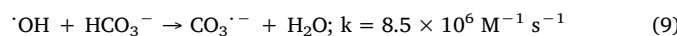
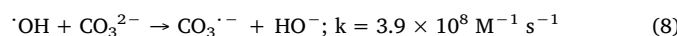
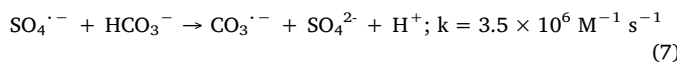


Fig. 6. Influence of different factors on BPA degradation. (a) pH; (b) HA; (c) Cl^- ; and (d) HCO_3^- and CO_3^{2-} (d). Reaction conditions: $[PS] = 5 \text{ mM}$, $[CFTS] = 1 \text{ g L}^{-1}$, $[BPA] = 0.1 \text{ mM}$, 25°C .



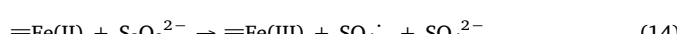
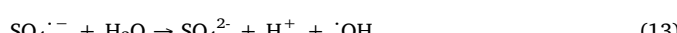
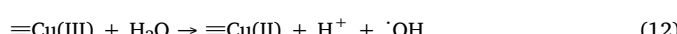
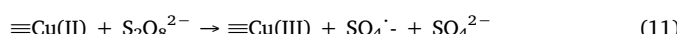
3.5. Treatment of actual wastewaters by CFTS

The actual phenol-acetone production wastewater was used to test the mineralization ability of the CFTS/PS system. The wastewaters were diluted before the degradation experiment, and the measured TOC concentrations of the wastewaters were 69.1 mg L^{-1} (Table S1). The results are shown in Fig. S7, approximately 37.5% of TOC in the wastewaters was removed by the CFTS after 60 min, which was substantially higher than those for Cu_2S (14.5%), FeS (28.5%), and SnS_2 (12.8%). This result implies that the CFTS/PS system possessed an excellent performance and great potential for practical applications in the treatment of wastewater. Additionally, the BPA mineralization in CFTS/PS system was also higher than that of other SR-AOPs reported in the previous studies [6,7,45], which further suggested the excellent performance of CFTS for PS activation and pollutant degradation. This result may be attributed to the tandem synergistic effect of Cu/Fe/Sn in CFTS promoting the cycle between M^{n+} and $\text{M}^{(n+1)+}$ and efficiency of PS activation. Therefore, more $\text{SO}_4^{\cdot-}$ is generated via persulfate activation using M^{n+} . Furthermore, the activation of persulfate into $\text{SO}_5^{\cdot-}$ ($E = 1.1 \text{ V}$) and $\text{SO}_3^{\cdot-}$ ($E = 0.63 \text{ V}$) can be inhibited by the reduction of $\text{M}^{(n+1)+}$ to M^{n+} , which would increase the utilization efficiency of PS to produce $\text{SO}_4^{\cdot-}$ [46–48]. More detailed mechanism of these processes will be discussed in the following sections.

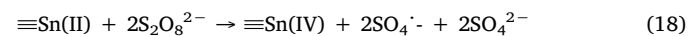
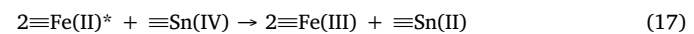
3.6. Mechanism of PS activation by CFTS

To investigate the catalytic mechanism of CFTS, the roles of the Cu and Fe in PS decomposition were studied. Similarly to CFTS, $\text{Cu}_2\text{ZnSnS}_4$ (CZTS) is regarded as being derived from the tetragonal structure of the corresponding MS species, in this case ZnS, in which there are eight atoms per primitive cell with body-centered tetragonal symmetry [49]. Therefore, we investigated the activity of a CZTS catalyst in which Fe^{2+} is substituted with the inactive Zn^{2+} . As shown in Fig. 7a, when the CFTS and PS are used together, BPA is totally degraded within 45 min. However, only 24.3% degradation is observed with CZTS for the same duration, indicating that more BPA is degraded by $\cdot\text{OH}$ and $\text{SO}_4^{\cdot-}$ produced from PS decomposition (Fig. 7b). During PS activation by the CZTS system, the surface $\equiv\text{Cu(I)}$ is oxidized to $\equiv\text{Cu(II)}$ accompanied by the generation of $\text{SO}_4^{\cdot-}$, and some of the generated $\text{SO}_4^{\cdot-}$ may be converted to $\cdot\text{OH}$ (Eqs. (10)–(13)) (Fig. 7c) [37]. When Fe is present in the system, i.e., when CFTS is used, the results are significantly improved, as shown in Fig. 4, indicating that $\equiv\text{Fe(II)}$ on the surface of CFTS is the main active site for PS decomposition.

According to our results and previous literature, $\equiv\text{Fe(III)}$ is thermodynamically likely to be reduced by $\equiv\text{Cu(I)}$, which is more conducive to the $\text{Fe(II)}/\text{Fe(III)}$ redox cycle (Eqs. 14 and 15) [15,21]. Thus, the synergistic effect of $\equiv\text{Cu(I)}$ and $\equiv\text{Fe(III)}$ on the surface of CFTS is benefit for interfacial electron transfer.



To explore the role of Sn(IV) in CFTS for PS decomposition, a series of combinations of Cu_2S , FeS , and SnS_2 were investigated. The potential synergistic effects of Sn and Fe were first confirmed. Theoretically, the reactivity of the FeS/SnS_2 system should be between those of SnS_2 and FeS , indicating that the BPA degradation in the presence of both FeS and SnS_2 should be never more than 64.5% after 45 min. However, the FeS/SnS_2 system performs better than both pure FeS and pure SnS_2 , as shown in Fig. 7d, suggesting that a synergistic effect between $\equiv\text{Fe(II)}$ and $\equiv\text{Sn(IV)}$ occurs during the activation of PS. Furthermore, in the PS decomposition system, Fe(III) ions are reduced via one-electron of Cu(I) and $\text{S}_2\text{O}_8^{2-}$, which result in the formation of Fe(II) ions. Some of the released Fe(II) ions are complexed with the 3s and 3p orbitals (sp^3 hybridized) of the surface S on CFTS via σ bonding ($\equiv\text{Fe(II)}^*$, Eq. (16)) [17]. The high valence metal like U^{VI} , Cr^{VI} , and As^{V} can be reduced by $\equiv\text{Fe(II)}^*$ as previously reported [21,50–53]. Similarly, $\equiv\text{Fe(II)}^*$ can reduce $\equiv\text{Sn(IV)}$ to $\equiv\text{Sn(II)}$ (Eq. (17)). $\equiv\text{Sn(II)}$ is also oxidized to $\equiv\text{Sn(IV)}$ by $\text{S}_2\text{O}_8^{2-}$ (Eq. (18)) [54]. The $\equiv\text{Fe(II)}^*$ formed plays a critical role in the tandem synergistic effect in the CFTS/PS system. In the $\text{Cu}_2\text{S}/\text{FeS}/\text{SnS}_2$ system, the degradation of BPA is enhanced when Cu_2S is added (Fig. 4d), further indicating that the advantage of the synergistic effect between $\equiv\text{Cu(I)}$ and $\equiv\text{Fe(III)}$. However, BPA removal efficiency of this mixture is still clearly lower than that of CFTS (Fig. 4d), probably owing to the formation of $\text{S}\rightarrow\text{M}$ σ -bonds ($\text{M} = \text{Cu}$, Fe , and Sn) that are beneficial to electron transfer.



XPS was employed to explore the primary functional sites and the surface valence states of fresh and used CFTS. As shown in Fig. S6c, the binding energy (BE) of $\text{Cu 2p}_{3/2}$ in fresh CFTS is 932.2 eV, suggesting that Cu(I) is the dominant Cu species [55]. After catalytic reaction, the area ratios for the $\text{Cu 2p}_{3/2}$ peaks is changed, showing that the relative content of Cu(I) increases from 63.1% to 69.5%, which is attributed to the $\equiv\text{Fe(II)}^*$ reduced $\equiv\text{Cu(II)}$ to $\equiv\text{Cu(I)}$ [21]. In Fe 2p spectra, the peak is corresponding to the $\text{Fe 2p}_{3/2}$ (712.0 eV) is in good agreement with the values of $\equiv\text{Fe(II)}$ [56]. Furthermore, there is no significant change in the $\text{Fe 2p}_{3/2}$ peak in used CFTS compared with that in the fresh catalyst (Fig. S6a, b). As shown in Fig. S6d, according to the characteristic BEs for the Sn(IV) (487.4 eV) and Sn(II) (486.5 eV) peaks in the $\text{Sn 3d}_{5/2}$ spectra, the relative content of Sn(IV) is decreased from 58.4% to 52.7%, which indicates that Sn(IV) can be reduced by $\equiv\text{Fe(II)}^*$ via the reaction in Eq. (17) [57]. The peaks in the S 2p spectrum are located at 161.4, 162.1, 163.0, 164.5 and 169.1 eV, which are assigned to S_2^{2-} , S^{2-} , S_n^{2-} , S° , and SO_4^{2-} , respectively (Table 1) [58–60]. The S^{2-} peaks for used CFTS is increased by 4% compared to that of the fresh catalyst, indicating that some of the S_2^{2-} and S_n^{2-} on the surface of CFTS is oxidized (Table 1). The S° peaks for used CFTS increases by 8% compared to that of the fresh catalyst, indicating that some S^{2-} is oxidized to S° and that Fe(II) is formed by the reaction in Eq. (19) [54]. These combined results indicate that Cu(II) and Sn(IV) on the CFTS surface are partially converted to Cu(I) and Sn(II) after the catalytic reaction.



3.7. Stability and reusability of CFTS

In order to study the stability and reusability of CFTS, reuse tests were conducted following reactions performed under the same conditions as those used above (Fig. S9). The degradation of BPA is maintained above 80% within 45 min over three reuse cycles. This indicates that BPA degradation over CFTS decreases only slightly with increasing use number. As shown in Fig. S8, the BET specific surface area of the

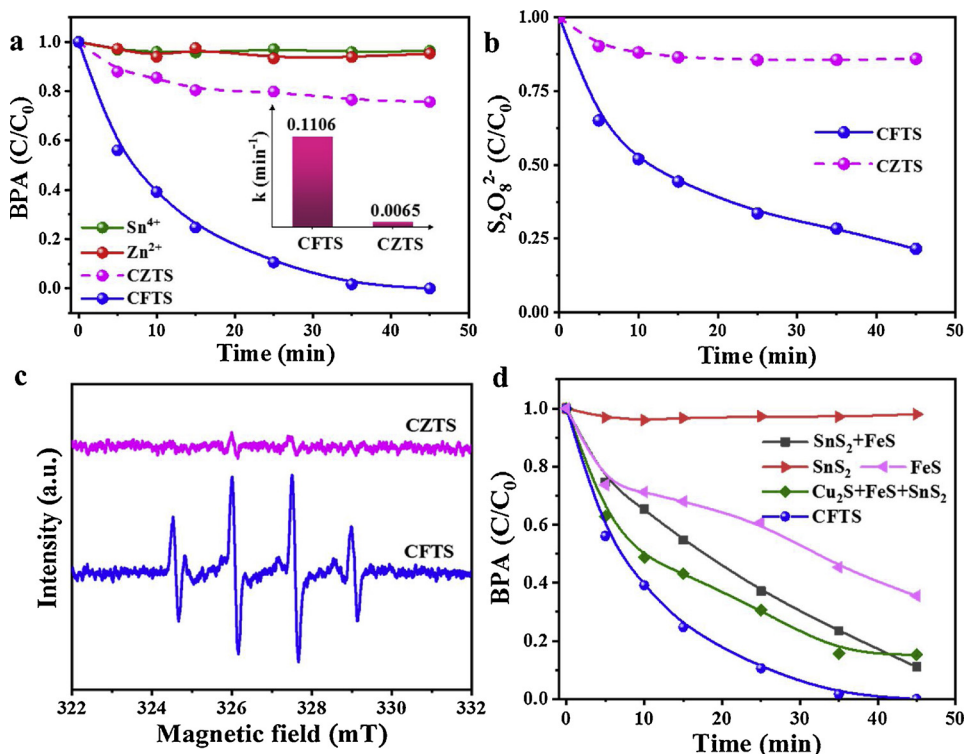


Fig. 7. (a) BPA degradation in catalytic PS oxidation with Zn²⁺, Sn⁴⁺, CZTS, or CFTS as the catalysts. Inset shows the rate constants of the CZTS and CFTS systems. (b) Impact of different systems on persulfate decomposition. (c) ESR spectra in the activation of PS in different systems (CZTS or CFTS). (d) BPA degradation in catalytic PS oxidation with various catalysts. Reaction conditions: [PS] = 5 mM, [catalyst] = 1 g L⁻¹, [BPA] = 0.1 mM, 25 °C.

Table 1
S 2p XPS results for the CFTS samples.

CFTS sample	S 2p binding energy (eV)				relative intensity ratio
	S ₂ ²⁻ or S ²⁻	S ²⁻	S _n ²⁻	S ⁰	
Before reaction	161.4	162.1	163.0	164.5	27:24:45:4
After reaction	161.4	162.2	163.10	164.4	25:28:35:12

reused CFTS is 34.47 m² g⁻¹, which is clearly larger than that of fresh CFTS (25.75 m² g⁻¹). The XRD spectra in Fig. 8b confirm that the reused CFTS maintains a stannite crystal structure, and the peaks below 30° could be due to the formation of insoluble carbonate and sulfate contaminants on the CFTS surface, partially covering the active sites and thus causing slight deactivation of the CFTS [61].

Metal leaching is usually a problem of concern in the PS activation by nanoscale metal-minerals or oxides, which was ascribed to the decomposition of PS produces H⁺ [32,61]. Therefore, the leaching of Cu, Sn, and Fe ions from the CFTS for different systems was monitored. For the CFTS/PS system, the concentrations of leached Cu, Fe, and Sn ions are 16.70, 1.36, and 0.057 mg L⁻¹, respectively (Table S2). But the

leached metal ions only contributed to 5% of BPA removal, confirming that the BPA degradation is a heterogeneous process that proceeds over the CFTS surface (Fig. 8a). Additionally, compared with other metal mineral/PS system such as Cu₂S/PS system, the Cu leaching from CFTS is considerably lower than that in the Cu₂S/PS system (131.60 ppm) (Table S2), indicating that a tandem synergistic effect between Cu, Fe, and Sn inhibits the leaching of Cu ions. To further solve the problem of Cu leached, the buffer solution (2 mM phosphate buffer, pH 7.0) was used to examine its effects on BPA degradation and Cu leached. As expected, the concentration of Cu leached was below the detection limit (< 0.05 mg/L), suggesting the completely inhibition of Cu leached, although the rate of BPA degradation (69.30%) was lower than that of without buffer (Fig. S9). Furthermore, the addition of HA also reduce the leached Cu concentration (Table S2), which indicated that metal leaching from the CFTS system can be effectively alleviated by some organic ligands in wastewater. Consequently, the well-controlled solution pH can solve the problem of metal leached when CFTS/PS system was used for the purification of wastewater.

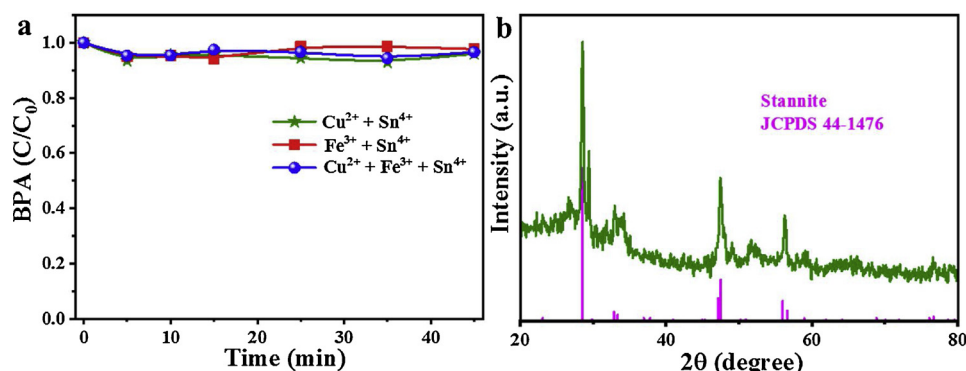


Fig. 8. (a) Effect of homogeneous catalysis on BPA degradation. (b) XRD pattern of reused CFTS.

4. Conclusions

CFTS nanoflowers were prepared by a facile hydrothermal approach. CFTS shows high activity and stability in catalytic activation of PS for BPA degradation and is more effective than monometallic Cu, Fe, and Sn sulfides. Both sulfate and hydroxyl radicals play key roles in BPA degradation. BPA is degraded through a surface catalytic process upon reaction with SO_4^{2-} and $\cdot\text{OH}$ generated in solution via PS activation. CFTS can be used over a wide range of pH conditions. The $\equiv\text{Fe}(\text{II})^*$ formed plays a critical role in the tandem synergistic effects of the CFTS/PS system. This effect leads to CFTS exhibiting high activity and stability in the activation of PS for BPA degradation. The tandem synergistic effect of Cu/Fe/Sn inhibit the leaching of metal ions by promoting the cycle between M^{n+} and $\text{M}^{(n+1)+}$. Thus, this study presents a low cost and promising mineral catalyst for the activation of PS in contaminant removal and provides new insight into the design and development of polymetallic catalyst for AOP technology.

Acknowledgments

This work was supported by the National Natural Science Foundation of China (Grant Nos. 21876099, 21750110438, and 21575077), the Science and Technology Development Plans of Shandong Province (ZR2017ZC0227) and the Fundamental Research Funds of Shandong University (2016JC030).

Appendix A. Supplementary data

Supplementary material related to this article can be found, in the online version, at doi:<https://doi.org/10.1016/j.apcatb.2019.04.069>.

References

- [1] Y. Zhang, W. Cui, W. An, L. Liu, Y. Liang, Y. Zhu, *Appl. Catal. B* 221 (2018) 36–46.
- [2] Y. Kawagishi, Y. Fujita, I. Kishi, I. Fukunaga, *J. Environ. Monit.* 5 (2003) 269–274.
- [3] D.M. Reif, M.T. Martin, S.W. Tan, K.A. Houck, R.S. Judson, A.M. Richard, T.B. Knudsen, D.J. Dix, R.J. Kavlock, *Environ. Health Perspect.* 118 (2010) 1714–1720.
- [4] S. Waclawek, H.V. Lutze, K. Grübel, V.V.T. Padil, M. Černík, D.D. Dionysiou, *Chem. Eng. J.* 330 (2017) 44–62.
- [5] W.D. Oh, Z. Dong, T.T. Lim, *Appl. Catal. B* 194 (2016) 169–201.
- [6] Y. Liu, R. Luo, Y. Li, J. Qi, C. Wang, J. Li, X. Sun, L. Wang, *Chem. Eng. J.* 347 (2018) 731–740.
- [7] R. Luo, C. Liu, J. Li, J. Wang, X. Hu, X. Sun, J. Shen, W. Han, L. Wang, *J. Hazard. Mater.* 329 (2017) 92–101.
- [8] G.X. Huang, C.Y. Wang, C.W. Yang, P.C. Guo, H.Q. Yu, *Environ. Sci. Technol.* 51 (2017) 12611–12618.
- [9] T. Olmez-Hancı, I. Arslan-Alaton, *Chem. Eng. J.* 224 (2013) 10–16.
- [10] G.P. Anipsitakis, D.D. Dionysiou, *Appl. Catal. B* 54 (2004) 155–163.
- [11] O.S. Furman, A.L. Teel, R.J. Watts, *Environ. Sci. Technol.* 44 (2010) 6423–6428.
- [12] R.H. Waldemer, P.G. Tratnyek, R.L. Johnson, J.T. Nurmi, *Environ. Sci. Technol.* 41 (2007) 1010–1015.
- [13] J. Wang, S. Wang, *Chem. Eng. J.* 334 (2018) 1502–1517.
- [14] J. Li, Y. Ren, F. Ji, B. Lai, *Chem. Eng. J.* 324 (2017) 63–73.
- [15] Y. Feng, D. Wu, Y. Deng, T. Zhang, K. Shih, *Environ. Sci. Technol.* 50 (2016) 3119–3127.
- [16] Y. Huang, C. Han, Y. Liu, M.N. Nadagouda, L. Machala, K.E. O'Shea, V.K. Sharma, D.D. Dionysiou, *Appl. Catal. B* 221 (2018) 380–392.
- [17] D.J. Vaughan, J.R. Craig, *Mineral Chemistry of Metal Sulfides*, Syndics of the Cambridge University Press, New York, 1978.
- [18] S. Chatterjee, A.J. Pal, *Sol. Energy Mater. Sol. Cells* 160 (2017) 233–240.
- [19] R.R. Prabhakar, N. Huu Loc, M.H. Kumar, P.P. Boix, S. Juan, R.A. John, S.K. Batabyal, L.H. Wong, *ACS Appl. Mater. Interfaces* 6 (2014) 17661–17667.
- [20] L. Ai, J. Jiang, *J. Mater. Chem.* 22 (2012) 20586–20592.
- [21] C. Dai, X. Tian, Y. Nie, H.M. Lin, C. Yang, B. Han, Y. Wang, *Environ. Sci. Technol.* 52 (2018) 6518–6525.
- [22] Y. Wang, H. Zhao, M. Li, J. Fan, G. Zhao, *Appl. Catal. B* 147 (2014) 534–545.
- [23] C. An, K. Tang, G. Shen, C. Wang, L. Huang, Y. Qian, *Mater. Res. Bull.* 38 (2003) 823–830.
- [24] L. Kong, G. Fang, Y. Kong, M. Xie, V. Natarajan, D. Zhou, J. Zhan, *J. Hazard. Mater.* 357 (2018) 109–118.
- [25] C. Liang, C.F. Huang, N. Mohanty, R.M. Kurakalva, *Chemosphere* 73 (2008) 1540–1543.
- [26] L. Kong, G. Fang, Y. Kong, M. Xie, V. Natarajan, D. Zhou, J. Zhan, *J. Hazard. Mater.* 357 (2018) 109–118.
- [27] Y. Zhu, M. Yue, V. Natarajan, L. Kong, L. Ma, Y. Zhang, Q. Zhao, J. Zhan, *RSC Adv.* 8 (2018) 14879–14887.
- [28] Y. Xie, P. Li, Y. Zeng, X. Li, Y. Xiao, Y. Wang, Y. Zhang, *Chem. Eng. J.* 335 (2018) 728–736.
- [29] C. Zhu, F. Zhu, C. Liu, N. Chen, D. Zhou, G. Fang, J. Gao, *Environ. Sci. Technol.* 52 (2018) 8548–8557.
- [30] G.-D. Fang, D.D. Dionysiou, D.-M. Zhou, Y. Wang, X.-D. Zhu, J.-X. Fan, L. Cang, Y.-J. Wang, *Chemosphere* 90 (2013) 1573–1580.
- [31] G. Fang, C. Liu, J. Gao, D.D. Dionysiou, D. Zhou, *Environ. Sci. Technol.* 49 (2015) 5645–5653.
- [32] G. Fang, W. Wu, C. Liu, D.D. Dionysiou, Y. Deng, D. Zhou, *Appl. Catal. B* 202 (2017) 1–11.
- [33] Y. Feng, P.-H. Lee, D. Wu, K. Shih, *Water Res.* 120 (2017) 12–21.
- [34] H. Li, J. Shang, Z. Yang, W. Shen, Z. Ai, L. Zhang, *Environ. Sci. Technol.* 51 (2017) 5685–5694.
- [35] X. Hou, X. Huang, F. Jia, Z. Ai, J. Zhao, L. Zhang, *Environ. Sci. Technol.* 51 (2017) 5118–5126.
- [36] H. Xu, D. Wang, J. Ma, T. Zhang, X. Lu, Z. Chen, *Appl. Catal. B* 238 (2018) 557–567.
- [37] P. Devi, U. Das, A.K. Dalai, *Sci. Total Environ.* 571 (2016) 643–657.
- [38] Tim K. Lau, Wei Chu, N.J.D. Graham, *Environ. Sci. Technol.* 41 (2007) 613–619.
- [39] X. Duan, C. Su, L. Zhou, H. Sun, A. Suvorova, T. Odedairo, Z. Zhu, Z. Shao, S. Wang, *Appl. Catal. B* 194 (2016) 7–15.
- [40] X. Duan, Z. Ao, L. Zhou, H. Sun, G. Wang, S. Wang, *Appl. Catal. B* 188 (2016) 98–105.
- [41] X. He, A.A. de la Cruz, D.D. Dionysiou, *J. Photochem. Photobiol. A: Chem.* 251 (2013) 160–166.
- [42] Y. Yang, J.J. Pignatello, J. Ma, W.A. Mitch, *Water Res.* 89 (2016) 192–200.
- [43] S. Khan, X. He, J.A. Khan, H.M. Khan, D.L. Boccelli, D.D. Dionysiou, *Chem. Eng. J.* 318 (2017) 135–142.
- [44] J.A. Khan, X. He, H.M. Khan, N.S. Shah, D.D. Dionysiou, *Chem. Eng. J.* 218 (2013) 376–383.
- [45] Y. Du, W. Ma, P. Liu, B. Zou, J. Ma, *J. Hazard. Mater.* 308 (2016) 58–66.
- [46] P. Devi, U. Das, A.K. Dalai, *Sci. Total Environ.* 571 (2016) 643–657.
- [47] G.P. Anipsitakis, D.D. Dionysiou, *Environ. Sci. Technol.* 38 (2004) 3705–3712.
- [48] W.-D. Oh, Z. Dong, T.-T. Lim, *Appl. Catal. B* 194 (2016) 169–201.
- [49] C. Huang, Y. Chan, F. Liu, D. Tang, J. Yang, Y. Lai, J. Li, Y. Liu, *J. Mater. Chem. A Mater. Energy Sustain.* 1 (2013) 5402–5407.
- [50] S. Chakraborty, F. Favre, D. Banerjee, A.C. Scheinost, M. Mullet, J.J. Ehrhardt, J. Brendle, L. Vidal, L. Charlet, *Environ. Sci. Technol.* 44 (2010) 3779–3785.
- [51] A.G. Williams, M.M. Scherer, *Environ. Sci. Technol.* 35 (2001) 3488–3494.
- [52] D.E. Latta, J.E. Bachman, M.M. Scherer, *Environ. Sci. Technol.* 46 (2012) 10614–10623.
- [53] F.S. Islam, A.G. Gault, C. Boothman, D.A. Polya, J.M. Charnock, D. Chatterjee, J.R. Lloyd, *Nature* 430 (2004) 68–71.
- [54] R. Rich, *Inorganic Reactions in Water*, Springer, Berlin Heidelberg, 2007.
- [55] NIST XPS Database - Cu 2p3/2.is a website :https://srdata.nist.gov/xps/EngElmSrchQuery.aspx?EType=PE&CSOpt=Retri_ex_dat&Elm=Cu.
- [56] X. Meng, H. Deng, J. Tao, H. Cao, X. Li, L. Sun, P. Yang, J. Chu, *J. Alloys. Compd.* 680 (2016) 446–451.
- [57] C. Di, G. Shen, K. Tang, S. Lei, H. Zheng, Y. Qian, *J. Cryst. Growth* 260 (2004) 469–474.
- [58] L. Guo, F. Chen, X. Fan, W. Cai, J. Zhang, *Appl. Catal. B* 96 (2010) 162–168.
- [59] H. Chen, Z. Zhang, Z. Yang, Q. Yang, B. Li, Z. Bai, *Chem. Eng. J.* 273 (2015) 481–489.
- [60] Y. Su, D. Jassby, S. Song, X. Zhou, H. Zhao, J. Filip, E. Petala, Y. Zhang, *Environ. Sci. Technol.* 52 (2018) 6466–6475.
- [61] X. Duan, C. Su, J. Miao, Y. Zhong, Z. Shao, S. Wang, H. Sun, *Appl. Catal. B* 220 (2018) 626–634.